Topological defects and nonhomogeneous melting of large two-dimensional Coulomb clusters

Minghui Kong, B. Partoens, and F. M. Peeters*
Departement Natuurkunde, Universiteit Antwerpen (UIA), Universiteitsplein 1, B-2610 Antwerpen, Belgium
(Received 26 July 2002; published 27 February 2003)

The configurational and melting properties of large two-dimensional (2D) clusters of charged classical particles interacting with each other via the Coulomb potential are investigated through the Monte Carlo simulation technique. The particles are confined by a harmonic potential. For a large number of particles in the cluster ($N>150$), the configuration is determined by two competing effects, namely, the fact that in the center a hexagonal lattice is formed, which is the groundstate for an infinite 2D system, and the confinement that imposes its circular symmetry on the outer edge. As a result, a hexagonal Wigner lattice is formed in the central area while at the border of the cluster the particles are arranged in rings. In the transition region defects appear as dislocations and disclinations at the six corners of the hexagonal-shaped inner domain. Many different arrangements and types of defects are possible as metastable configurations with a slightly higher energy. The particle motion is found to be strongly related to the topological structure. Our results clearly show that the melting of the clusters starts near the geometry induced defects, and that three different melting temperatures can be defined corresponding to the melting of different regions in the cluster.

DOI: 10.1103/PhysRevE.67.021608 PACS number(s): 61.72.−y, 45.05.+x, 61.46.+w, 73.22.−f

I. INTRODUCTION

Recently, there has been considerable theoretical and experimental progress in the study of mesoscopic systems consisting of a finite number of charged particles which are confined into an artificial circular symmetric potential. Typical experimental model systems for the study of this system are electrons on the surface of liquid helium [1], electrons in quantum dots [2], colloidal suspensions [3,4] and in confined plasma crystals [5]. Colloidal particles dissolved in water [6] are another example of an experimental system where classical particles exhibit Wigner crystallization. Recently, macroscopic two-dimensional (2D) Wigner islands consisting of charged metallic balls above a plane conductor were studied, and the ground state, metastable states, and saddle point configurations were found experimentally [7].

Such a system with a finite number of particles, initially studied by Thomson as a classical model for the atom [8,9], has been extensively studied during the past few years. For a small number of particles (typically $N<100$), they are arranged in rings [10–13] and a Mendeleev-type of table was constructed in Ref. [11], which gives the distribution of those particles over the different rings. Moreover, the configurations of the ground-state, metastable states, and saddle point states were obtained, from which the transition path and the geometric properties of the energy landscape were given in Ref. [14]. The spectral properties of the ground state configurations were presented in Ref. [12] and generalized to screened Coulomb [15,16] and logarithmic [9,16] interparticle interactions. The excitation of the normal modes of 2D Coulomb clusters in laboratory complex plasmas were recently observed [17].

The melting properties of this system have been studied experimentally [6,18] and by Monte Carlo (MC) [19,20] and molecular dynamics [21,22] simulations. In a hard wall confined system with short-range interparticle interaction, the melting behavior was found even more interesting. Reentrant melting of 2D colloidal clusters in a hard wall potential was obtained in both experimental [6] and theoretical work [21].

The defect structure in crystals is of paramount importance for the stability and the strength of materials. Topological defects in Wigner crystals [23,24] and their effect on particle melting were investigated in Refs. [18,19,22,25]. Thermal defect mediated melting was proposed as the microscopic mechanism for melting in an infinite 2D triangular Wigner crystal.

In this paper we study topological defects that are induced by the confinement potential, i.e., which are a result of the finite size of the system. Next we investigate how these defects influence the melting of the mesoscopic 2D island. The present paper is organized as follows. In Section II, we describe the model system and the numerical approach. Sec. III is devoted to the structural properties of the topological defects at zero temperature. In Sec. IV, we discuss the eigenmode spectrum for these large clusters. The discussion on the nonhomogeneous melting is presented in Sec. V. Our conclusions are given in Sec. VI.

II. NUMERICAL APPROACH

The model system was defined in Ref. [11] and the Hamiltonian for such a system is given by

$$H=\frac{q^2}{\varepsilon}\sum_{i>j}^{N}\frac{1}{|\hat{r}_i-\hat{r}_j|}+\sum_{i}^{N}V(\hat{r}_i). \tag{1}$$

The confinement potential $V(\vec{r})=\frac{1}{2}m^*\omega_0^2r^2$ is taken to be circular symmetric and parabolic, where m^* is the effective mass of the particles, q is the particle charge, ω_0 is the radial confinement frequency, and ε is the dielectric constant of the medium the particles are moving in. To exhibit the scaling of the system, we introduce the character-

*Email address: peeters@uia.ua.ac.be

istic scales in the problem: $r_0=(2q^2/m\epsilon\omega_0^2)^{1/3}$ for the length, $E_0=(m\omega_0^2q^4/2\epsilon^2)^{1/3}$ for the energy, and $T_0=(m\omega_0^2q^4/2\epsilon^2)^{1/3}k_B^{-1}$ for temperature. After the scaling transformations $(r\rightarrow r/r_0, E\rightarrow E/E_0, T\rightarrow T/T_0)$, the Hamiltonian can be rewritten in a simple dimensionless form as

$$H=\sum_{i>j}^{N}\frac{1}{|\hat{r}_i-\hat{r}_j|}+\sum_{i}^{N}r_i^2, \tag{2}$$

which only depends on the number of particles N. The numerical values for the parameters $\omega_0, r_0, E_0, T_0$for some typical experimental systems were given in Ref. [11].

The MC simulation technique [26] is relatively simple and rapidly convergent and it provides a reliable estimation of the total energy of the system in cases when relatively small number of Metropolis steps are sufficient. However, the accuracy of this method in calculating the explicit states is poor for systems with a large number of particles, which have significantly more metastable states. To circumvent this problem we employed the Newton optimization technique after the standard MC routine. This procedure was outlined and compared with the standard MC technique in Ref. [12]. The structure and potential energies of the system at $T\neq 0$ are found by the standard Metropolis algorithm [26], in which at some temperature the next simulation state of the system is obtained by a random displacement of one of the particles. We allow the system to approach its equilibrium state at some temperature T, after executing 10^4–(5×10^5) MC steps. Each MC step is formed by a random displacement of all particles. If the new configuration has a smaller energy it is accepted, but if the new energy is larger the configuration is accepted with probability $\delta<\exp(-\Delta E/T)$, where δ is a random number between 0 and 1 and ΔE is the increment in the energy [19].

III. TOPOLOGICAL DEFECTS

It is well known that the hexagonal lattice is the most energetically favored structure for classical point charges in a two-dimensional infinite plane at low temperature [27]. For a system consisting of a finite number of repelling particles restricted to 2D, which are held together by a circular harmonic potential, the cluster patterns are determined by the need to balance the tendency to form a triangular lattice against the formation of a compact circular shape. The configuration is determined by these two competing effects, namely, circular symmetry and triangular structure (Wigner lattice). This competition leads to intrinsic defects in the 2D circular Coulomb cluster, which are *geometry* (of the confinement potential) *induced defects*. This ground state is not a defect-free system. The symmetry breaking is due to the packing of the triangular lattice into a region with a circular boundary. A hexagonal lattice that is cut by a circle without the introduction of any defect has an energy $E=56.0499E_0$ that is larger than the ground-state energy $E=55.9044E_0$ for $N=291$ particles.

In the first part of this paper, we investigate the form and position of the defects in large clusters. Therefore we make use of the Voronoi construction [28]. The Voronoi construction of a collection of particles consists of a partition of space into cells. Each cell consists of those points that are closer to the given particular particle than to any other particle. Examples of Voronoi constructions are shown in Fig. 1, where the ground-state configurations for $N=291$, 300, 400, and 500 are shown. One can see that there are two kinds of defects, i.e., dislocations and disclinations. Disclinations are orientational defects with a fivefold (indicated by –) or sevenfold (indicated by +) coordination number (the number of sides of the polygon around the particles is nothing else but the coordination number). A dislocation is a pair of two disclinations consisting of a defect with a fivefold (–) and a defect with a sevenfold (+) coordination number. In the latter case the ordering at long distances is not disrupted and consequently such a bound pair has a much lower energy [29]. The total number of fivefold N_- and sevenfold N_+ disclinations depends on the particular configuration. The number of disclinations in this system is determined by Euler's theorem and can not be changed, so the net topological charge N_--N_+ is always equal to 6 as was already demonstrated in Refs. [16,30]. The reason is that every – defect can bend the lattice clockwise over $\pi/3$ from a straight lattice and thus six – defects can bend a straight line into a circle. Dislocations will appear when it decreases the energy of the system. From Fig. 1 it is apparent that this is more so for larger clusters.

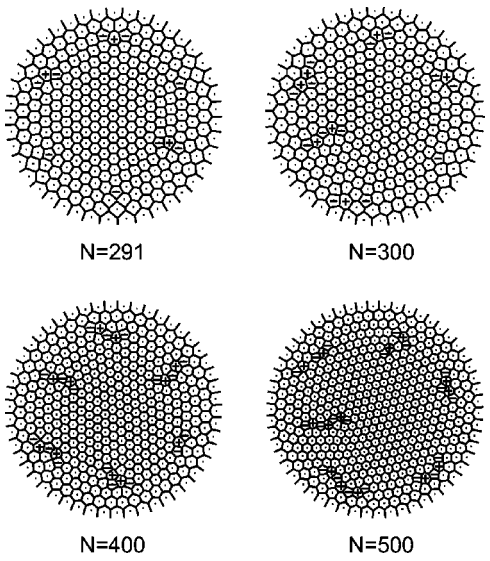

FIG. 1. The ground-state configurations for $N=291$, 300, 400, 500 particles. The Voronoi structure is shown and the defects (i.e., disclinations) are indicated by + for a sevenfold and by - for a fivefold coordination number.

In Refs. [16,22], the defects in clusters with a logarithmic interparticle interaction were studied. We want to stress that their way of visualizing the defects is different: nearest neighbors are connected by a line, without making crossings. However, this does not lead to a unique picture: the total number of fivefold, N_-, and sevenfold, N_+, disclinations can vary in the same configuration, only the net topological charge N_--N_+ is always equal to 6.

In these large clusters, the defects are located on a hexa-

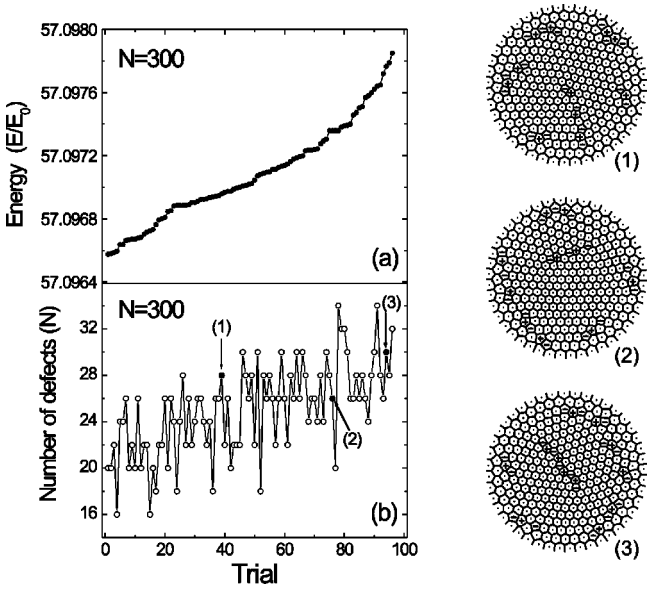

FIG. 2. The energy E/E_0 (a) and the total number of defects (b) of different metastable states are shown for $N=300$. Three typical defect configurations with different energies are shown on the right side of the figure.

gon, i.e., they form a hexagonal structure. As can be seen in Fig. 1, the defects are approximately situated at the six corners of a hexagon, each corner with a net topological charge of -1. Notice from Fig. 1 that a single fivefold disclination can appear, but never a single sevenfold disclination. For the large strain energy around the -1 topological charge, some dipole defects (i.e., dislocations with -1 and $+1$ defects) will be generated to shield the -1 topological charge. These shielding dipole defects do not change the topology of the system. A clearer example is shown in the inset of Fig. 7(b) for the $N=291$ ground-state configuration. We considered the $N=291$ system as it minimizes the number of defects. The reason is that, for this particle number the configuration has 42 particles in the outer ring, which is a multiple of the topological charge. There are three rings at the border with an equal number ($N=42$) of particles (the 1D Wigner lattice), the central hexagonal structure (the 2D Wigner lattice) and the defects indicated by triangles ($\triangle$) and squares ($\square$) are situated (i) around the six corners of a hexagon and (ii) in the transition region between the outer rings and the central hexagon.

It should be noted that the search for the global minimum configuration is a difficult problem for large systems because of the existence of a large number of local-minimum configurations, with energy very close to the global minimum. Thus one is never absolutely sure to have found the real ground state. Therefore, we investigated the different metastable states. In an experiment, these metastable states may be reached by thermal excitation if the energy barrier between them and the ground state is comparable to or smaller than k_BT. The saddle points between these metastable states were investigated in an earlier paper [14] for $N\leqslant 20$. In Fig. 2 the energy and the total number of defects of different metastable states are shown for $N=300$. The results for the different metastable configurations are ordered with increasing energy. Note from Fig. 2(b) that on average the total number of defects increases with energy, but it shows strong local variations. Only an even number of defects are obtained, because the net topological charge is always 6, and the dipole defects (i.e., one dislocation with -1 and $+1$ defects) always appear in pairs. Also the hexagonal position of the defects disappears [see enlargement (1) in Fig. 2] and more free dislocations are found. These defects move from the transition region to the border [see enlargement (2) in Fig. 2] or to the central region [see enlargement (3) in Fig. 2]. For configurations with higher energies, the defects arrange themselves in long chains, i.e., dislocation lines. On average the configurations with defects on the border have a lower energy than those with defects in the center.

We also investigated whether or not it is possible to have a configuration with only six fivefold disclinations and no other defects (for example for the $N=85$ configuration with 24 particles on the outermost ring [30]). Therefore, we started our MC procedure with a perfect hexagonal structure without any defect and then allowed it to relax to its energy minimum. We did this for $N=281$ up to 295 particles, because we noted that for these particle numbers the configuration has about 42 particles in the outer ring, which is a multiple of 6, i.e., the net topological charge. Only in such a case one can have the situation in which just six fivefold disclinations are present. We found that our result (from $N=281$ up to 295 particles) never converges to a configuration with only six fivefold disclinations. However, this procedure indeed favorably relaxes to configurations with 42 particles on the outer ring, often resulting in a configuration that has less total number of defects than the corresponding ground state.

IV. THE EIGENMODE SPECTRUM

The effect of the geometry induced defects on the eigenfrequencies (i.e., the eigenmode spectrum) were also investigated for these large clusters. In this system, it is well known that there are three eigenfrequencies that are independent of N [12]: $\omega=0,\sqrt{2}$, and $\sqrt{6}$, which correspond to the rotation of the system as a whole, the center of mass mode, and the breathing mode, respectively. The above modes were recently observed experimentally [17]. The smallest frequency no longer corresponds to intershell rotation as in small clusters [12] but to the excitation of a vortex-antivortex pair, of which a typical mode is shown in Fig. 3(a). Slightly larger excitation energies may consist of multiples of such pairs [see Fig. 3(b)]. Modes with higher eigenfrequencies often show a hexagonal structure similar to the ordering of the defects. The motion can be concentrated around [see Fig. 3(c)] or between the defects [see Fig. 3(d)]. The local modes can be found at the six corners of the hexagon where the defects are exactly situated [see Fig. 3(e)]. The modes in which the inner particles have larger amplitudes than the outer particles have the largest eigenfrequencies [see Fig. 3(f)].

The lowest eigenfrequencies of the excitation spectrum corresponding to the ground-state configuration of the sys-

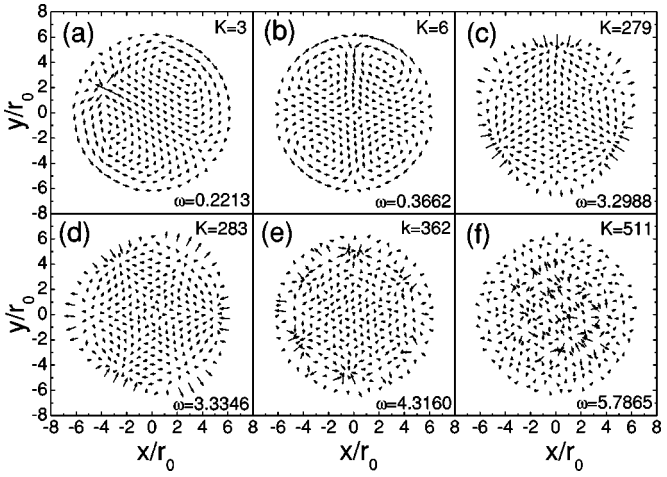

FIG. 3. Vector plot of the eigenvectors for the cluster with $N=291$ particles for six different values of the mode number K.

tem is shown in Fig. 4, as a function of the number of particles for N ranging from 281 to 307. The labels in Fig. 4 denote the total number of defects present in the ground state. Notice that only an even number of defects are obtained as explained before. On average, configurations with a large number of defects have a smaller lowest eigenfrequency and are thus less stable, and vice versa.

In this 2D lattice, all behaviors of the cluster modes can be classified as shearlike or compressionlike modes. In order to characterize the compressional and shear parts of these eigenmodes, we calculated, respectively, the divergence $\vec{\nabla}\cdot\vec{v}$ and the vorticity $(\vec{\nabla}\times\vec{v})_z$ of the velocity field. To calculate the velocity field, we interpolated the displacements of Fig. 3 on a 100×100 grid (thus neglecting the constant eigenfrequency). The divergence and vorticity maps were then calculated at every point of this matrix. Notice that pure

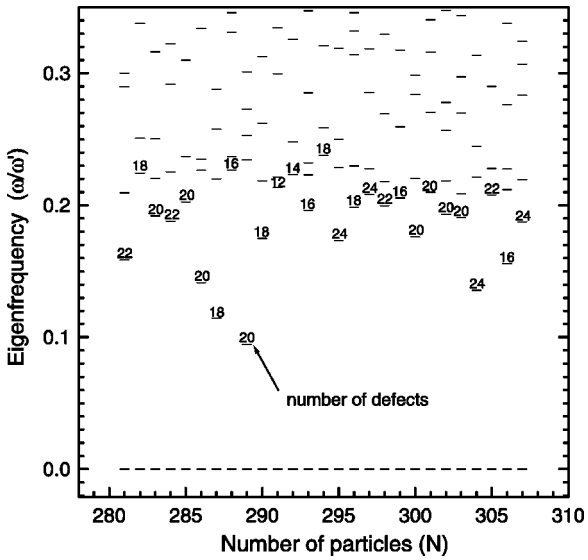

FIG. 4. Excitation spectrum of normal modes as a function of the number of particles in the cluster. The frequency is in units of $\omega'=\omega_0/2^{1/2}$. The numbers in the figure indicate the number of defects found in the ground states of the different clusters.

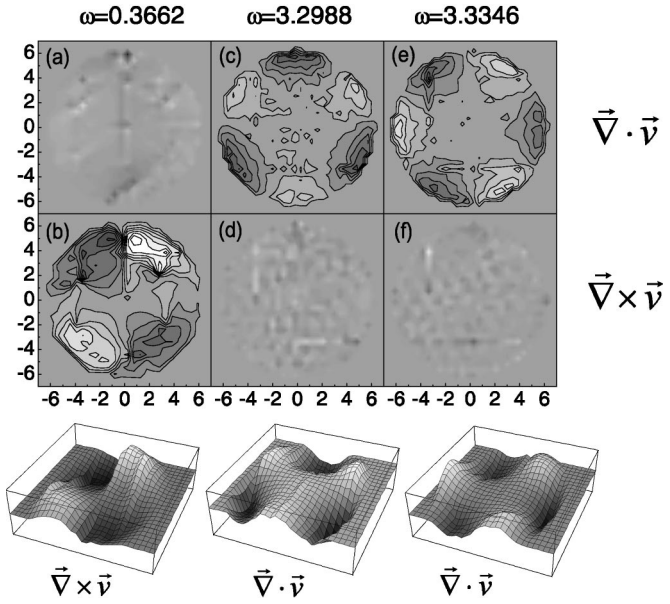

FIG. 5. Gray-scale contour maps of the vorticity $(\vec{\nabla}\times\vec{v})_z$ and the divergence $\vec{\nabla}\cdot\vec{v}$ of the velocity field of three different eigenmodes. A corresponding 3D plot is shown for those maps that exhibit a clear structure.

shear or compressional modes do not exist in the circular boundary of finite cluster. Figure 5(b) shows the vorticity and thus displays the shear part of the eigenmode of Fig. 3(b). The two vortex-antivortex pairs are clearly seen. The divergence map for this eigenmode is practically zero everywhere, as there is no compressional part [Fig. 5(a)]. This is not the case for the eigenmodes (c) and (d) of Fig. 3. Figures 5(c) and 5(e) show the divergence maps for both eigenmodes, in which the compression and rarefaction can be clearly seen. Both cases show no shear part [Figs. 5(d) and 5(f)]. Figures 5(c) and 5(e) (see also the 3D plots at the bottom of Fig. 5) exhibit clearly dipole type of compressional oscillations between [Fig. 5(c)] and at [Fig. 5(e)] the defect regions.

V. NONHOMOGENEOUS MELTING

Understanding the microscopic mechanism of melting has intrigued scientists since the late nineteenth century. Special interest has been devoted to 2D melting [31]. Most works address infinite systems consisting of a single layer. However, whether melting of a 2D crystal is a first-order transition and proceeds discontinuously or is a continuous transition in which the crystal first transits into a hexatic phase retaining quasi-long-range orientational order and then melts into an isotropic fluid is still an open question and a controversial issue.

In the present work we consider a finite 2D system where we take $N=291$ for our numerical simulation. Here we present a calculation of the melting phase diagram by performing MC simulations. In Ref. [22] molecular dynamics was used to investigate the melting of a cluster of particles interacting through a logarithmic interaction. As compared to our Coulomb interaction, where the geometry induced de-

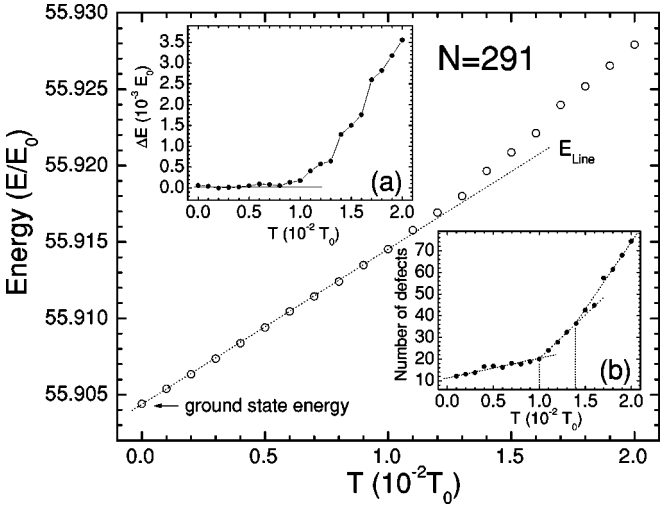

FIG. 6. The potential energy (E/E_0) of the 2D Coulomb cluster as a function of temperature T/T_0 for $N=291$. The insets show $\triangle E=E-E_{line}$ (a) and the number of defects (b) as a function of temperature T/T_0.

fects are situated in the third and fourth outer shells (i.e., the transition region) and around the six corners of the ''defect'' hexagon, in the logarithmic interacting system [22] these defects are mainly situated in the outer two shells. In Ref. [22], the number and type of defects were studied as a function of the noise (i.e., temperature). Here we will use several different criteria such as the total energy, the radial dependent mean square displacement, the bond-angular order factor, and the angular square deviation to characterize the melting behavior of the cluster.

There are several different criteria that can be used to find the melting temperature. In order to determine the melting transition point, we calculated the potential energy of the system as a function of temperature (see Fig. 6). In the crystalline state the potential energy of the system increases almost linearly with temperature, and then after the critical temperature is reached $(T/T_0=0.01$ for $N=291)$, it increases more steeply as shown in Fig. 6. This is a signature of melting and is related to the unbinding of dislocation pairs. The dotted assurgent line in Fig. 6 indicates the linear temperature dependence of the potential energy for low temperatures before melting. In the upper inset (a) of Fig. 6, we plot ΔE, which is the difference between the obtained numerical energy and the linear T behavior. After the melting point, ΔE increases superlinearly.

The lower inset (b) of Fig. 6, shows the averaged number of defects as a function of temperature T/T_0. The number of defects were obtained as follows. We considered 40 configurations for every temperature T/T_0. After every 500MC steps, a new configuration was obtained. For all these configurations the number of defects were counted. Finally we averaged over the 40 configurations, which is the reason why the number of defects can be noninteger. With increasing temperature, the system generates more and more defects and after the melting point the number of defects grows very fast. Notice that two clear critical temperatures emerge from this figure at the crossing points of the dotted lines, i.e.,

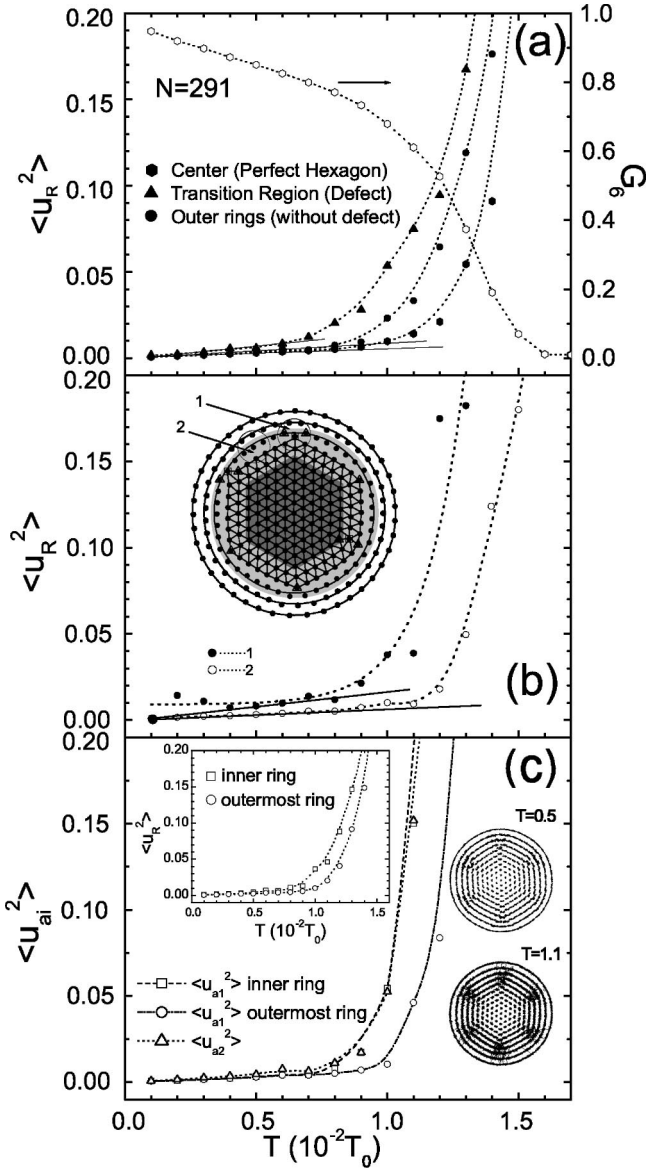

FIG. 7. (a) The mean square displacements as a function of the temperature T/T_0 for the three regions defined in the inset of (b) for $N=291$ particles. The open symbols are the results for the correlation function G_6 referred to on the right scale, for the inner hexagonal region. The linear dependence at low temperature is accentuated by the thin straight lines. The dotted curves are guides to the eye. (b) The mean square displacements as a function of the temperature T/T_0 for the small defect-free (open symbols) and defect regions (solid symbols) in the intermediate region as indicated by the circular areas in the inset. The thin straight lines show the low temperature linear dependence. The inset is the ground-state configuration for $N=291$. The dots give the position of the particles. Three regions are found: I (dark gray colored hexagonal area) is comprised of the defect-free hexagonal lattice, II is a transition region with the defects (light gray colored area), and III consists of the outermost two rings. The $+1$ and -1 topological defects are represented by the open squares and triangles, respectively. (c) The relative angular intrashell square deviation $\langle u_{a1}^2\rangle$ and relative intershell square deviation $\langle u_{a2}^2\rangle$ of the outermost two rings as a function of temperature for $N=291$.

$T/T_0=0.01$ and $T/T_0=0.014$.

On the right-hand side of Fig. 7(c) we plot typical particle trajectories for two temperatures, which show that the melting of this system is very complex and nonhomogeneous. The top figure shows the particle trajectories before melting, and the bottom figure shows the particle trajectories after melting. It clearly indicates that the melting starts around the six corners of the hexagon, which are exactly the defect regions. With increasing temperature, the particles in the defect region start to move radially and destroy order locally. With further increase of temperature the total system completely melts and the order is destroyed.

In order to better describe the spatial dependence of the melting process in our system, we separate the configuration into three regions as shown in the inset of Fig. 7(b). Region I (dark gray colored hexagonal area) is comprised of the defect-free hexagonal center, region II is a transition region with the defects (light gray colored area), and region III consists of the outermost two rings. For the case of $N=291$ particles, region I consists of 91 particles, region II consists of 116 particles, and region III consists of 84 particles. We calculate for each region the mean square displacement $\langle u_R^2\rangle$, which was introduced in Ref. [11],

$$\langle u_R^2\rangle=\frac{1}{N}\sum_{i=1}^{N}\langle(r_i-\langle r_i\rangle)^2\rangle/a^2, \tag{3}$$

with $a=2R/\sqrt{N}$ the average distance between the particles. Figure 7(a) shows $\langle u_R^2\rangle$ as a function of the reduced temperature T/T_0 for the three different regions. At low temperatures the particles exhibit harmonic oscillations around their $T=0$ equilibrium position, and the oscillation amplitude increases linearly and slowly with temperature: the particles are well localized and display still an ordered structure. This linear dependence is accentuated by the thin straight lines in Fig. 7(a). Here, we already notice that the amplitude of the local particle thermal vibrations in these different regions are different. The amplitude is largest at the defect region and lowest in the center of the cluster. Melting occurs when $\langle u_R^2\rangle$ increases very sharply with T. Because of the finite number of particles one has rather a melting region, instead of a well-defined melting temperature. After the melting point, the particles exhibit liquidlike behavior. Figure 7(a) exhibits three different melting temperatures corresponding to the three different regions. First, region II, i.e., the transition region containing the defects, starts to melt, then the outermost two rings melt, and finally the hexagonal region melts. Following Ref. [32], we can define a melting temperature at the point where $\langle u_R^2\rangle\approx 0.10$, which results in the melting temperatures $T_{melt}/T_0\simeq 0.0115$, 0.0125, and 0.0138 for the defect region, the outer rings, and the center region, respectively.

In order to investigate the melting in the defect region in further detail, we consider two new small regions as shown in the inset of Fig. 7(b). One region is around the defect, the other does not contain a defect and is situated between two defect regions. For $N=291$, each of the two regions contains, respectively, eight and seven particles. In Fig. 7(b), the $\langle u_R^2\rangle$ of these two different regions show a different melting temperature: the melting clearly starts first around the defect as expected. The particle motion is strongly influenced by the topological defects, i.e., the particles in the defect regions are less well interlocked and have a larger diffusion constant than the undistorted lattice regions, and it is easier to excite their thermal motions [25]. Notice that for the two separate regions a much sharper melting behavior is found than for the intermediate region as a whole [see Fig. 7(a)]. The reason of course is that in Fig. 7(a) one averages over defect and defect-free regions. The criterion $\langle u_R^2\rangle\approx 0.10$ results into $T_{melt}/T_0\simeq 0.0118$, and 0.0138 for the defect and the defect-free regions, respectively. These two melting temperatures are very similar to the melting temperature of the transition region and the hexagonal region of Fig. 7(a).

The third independent parameter is the bond-orientational correlation function. This quantity determines the type of melting transition and the melting point for an infinite system. Our finite system is too small in order to have a reliable analysis of the asymptotic decay of the density correlation function. Therefore, we calculate the bond-angular order factor that was originally presented in Ref. [33], but following Ref. [19] we modified it into

$$G_6=\left\langle\frac{1}{N}\sum_{j=1}^{N}\frac{1}{N_{nb}}\exp(iN_{nb}\theta_{j,n})\right\rangle. \tag{4}$$

This quantity is calculated only for region I, which exhibits a hexagon structure, where j means the N_{nb} nearest neighbors of particle i, for the ideal hexagonal lattice $N_{nb}=6$, where $\theta_{j,n}$ is the angle between some fixed axis and the vector that connects the j^{th} particle and its nearest n^{th} neighbor.

For a perfect hexagonal system, $G_6=1$. In our system, for $N=291$, the initial value of G_6 is 0.96, which means that the structure in region I is almost perfectly hexagonal. Our numerical results [see open dots in Fig. 7(a)] show that G_6 decreases linearly with increasing temperature. When G_6 is around 0.6, it more rapidly drops to zero with increasing temperature. G_6 should be zero for the liquid state. This can be compared with the infinite system where a universal melting criterion was found in Ref. [19]: melting occurs when the bond-angle correlation factor becomes $G_\theta\approx 0.45$, which was found to be independent of the functional form of the interparticle interaction. For our system the value $G_\theta\approx 0.45$ is probably not correct because in our finite system G_6 does not drop to zero at T_{melt}, but is smeared out around T_{melt}. Therefore, the midpoint $G_6\approx 0.45/2\approx 0.225$ is expected to describe better the melting temperature. This leads to $T_{melt}/T_0\simeq 0.0136$, which is similar to the result $T_{melt}/T_0\simeq 0.0138$ obtained from the radial displacement criterion.

In contrast to bulk systems, the melting scenario of small laterally confined 2D systems was found earlier [11] to be a two-step process. Upon increasing the temperature, the first intershell rotation becomes possible where orientational order between adjacent shells is lost while retaining their internal order and the shell structure. At even higher temperatures, the growth of thermal fluctuations leads to radial diffusion between the shells, which finally destroys the posi-

tional order. To characterize the relative angular intrashell and the relative angular intershell, we use the functions as defined in Ref. [11]. The relative angular intrashell square deviation

$$\langle u_{a1}^2 \rangle = \frac{1}{N_R} \sum_{i=1}^{N_R} [\langle (\varphi_i - \varphi_{i1})^2 \rangle - \langle \varphi_i - \varphi_{i1} \rangle^2] / \varphi_0^2 \quad (5)$$

and the relative angular intershell square deviation

$$\langle u_{a2}^2 \rangle = \frac{1}{N_R} \sum_{i=1}^{N_R} [\langle (\varphi_i - \varphi_{i2})^2 \rangle - \langle \varphi_i - \varphi_{i2} \rangle^2] / \varphi_0^2, \quad (6)$$

where i_1 indicates the nearest-particle from the same shell, while i_2 refers to the nearest-neighbor shell, $\varphi_0 = 2\pi/N_R$, where the number in the outermost two rings N_R is the same and equals 42 for our $N=291$ system. Only the two outermost rings have a clear shell structure. Both two outer rings are strongly interlocked, which is a consequence of the 1D Wigner lattice arrangement of the two rings. From the left inset of Fig. 7(c), one can see that the inner ring will melt before the outermost ring. We find that the result for $\langle u_{a1}^2 \rangle$ of the inner ring is almost the same as $\langle u_{a2}^2 \rangle$, which is the relative angular intershell square deviation. It means that when the inner ring loses its order, the relative order is lost simultaneously. The outermost ring can still keep its order and it will melt at even higher temperature. Comparing this with Fig. 7(a), we see that the radial and angular displacements start to increase rapidly at approximately the same temperature. Thus, for large clusters, intershell rotation will not occur below the melting temperature, but appears at the same temperature when the radial displacements increase.

VI. CONCLUSION

The configurational and melting properties of large two-dimensional clusters of charged classical particles interacting with each other via the Coulomb potential were investigated through the Monte Carlo simulation technique. For the ground-state configuration, a hexagonal Wigner lattice is formed in the central area while on the border of the cluster, the particles are arranged in rings. In the transition region between them, defects appear as groups of dislocations and disclinations at the six corners of the hexagonal-shaped inner domain. Many different arrangements and types of defects are possible as metastable configurations with a slightly higher energy. The particle motion is found to be strongly related to the local topological structure. Our results clearly show that the melting of the clusters starts near the geometry induced defects, and that three melting temperatures can be obtained: $T_{melt}/T_0 \simeq 0.0115$, 0.0125, and 0.0138 for the defect region, the outer rings and the center region, respectively. These values are for the $N=291$ cluster. Taking a different value for N does not lead to any qualitative differences, it only influences slightly the values for the three melting temperatures.

ACKNOWLEDGMENTS

This work was supported by the Flemish Science Foundation (FWO-Vl), the Belgian Inter-University Attraction Poles (IUAP-V), the ''Onderzoeksraad van de Universiteit Antwerpen''(GOA), and the EU Research Training Network on ''Surface Electrons on Mesoscopic Structures.'' We are very grateful to Dr. I. V. Schweigert for helpful discussions. Stimulating discussions with Professor A. Matulis, Ying-Ju Lai, and M. Milošević are gratefully acknowledged.

[1] C.C. Grimes and G. Adams, Phys. Rev. Lett. **42**, 795 (1979).
[2] R.C. Ashoori, Nature (London) **379**, 413 (1996).
[3] S. Neser, C. Bechinger, P. Leiderer, and T. Palberg, Phys. Rev. Lett. **79**, 2348 (1997).
[4] M. Golosovsky, Y. Saado, and D. Davidov, Phys. Rev. E **65**, 061405 (2002).
[5] J.H. Chu and L. I, Phys. Rev. Lett. **72**, 4009 (1994).
[6] R. Bubeck, C. Bechinger, S. Neser, and P. Leiderer, Phys. Rev. Lett. **82**, 3364 (1999).
[7] M. Saint Jean, C. Even, and C. Guthmann, Europhys. Lett. **55**, 45 (2001).
[8] J.J. Thomson, Philos. Mag. **7**, 237 (1904).
[9] B. Partoens and F.M. Peeters, J. Phys.: Condens. Matter **9**, 5383 (1997).
[10] F. Bolton and U. Rössler, Superlatt. Microstruct. **13**, 139 (1993).
[11] V.M. Bedanov and F.M. Peeters, Phys. Rev. B **49**, 2667 (1994).
[12] V.A. Schweigert and F.M. Peeters, Phys. Rev. B **51**, 7700 (1995).
[13] Yu.E. Lozovik and E.A. Rakoch, Phys. Rev. B **57**, 1214 (1998).
[14] M. Kong, B. Partoens, and F.M. Peeters, Phys. Rev. E **65**, 046602 (2002).
[15] L. Cândido, J.P. Rino, N. Studart, and F.M. Peeters, J. Phys.: Condens. Matter **10**, 11627 (1998).
[16] Y.J. Lai and L. I, Phys. Rev. E **60**, 4743 (1999).
[17] A. Melzer, M. Klindworth, and A. Piel, Phys. Rev. Lett. **87**, 115002 (2001); A. Melzer (unpublished).
[18] K. Zahn, R. Lenke, and G. Maret, Phys. Rev. Lett. **82**, 2721 (1999).
[19] I.V. Schweigert, V.A. Schweigert, and F.M. Peeters, Phys. Rev. Lett. **82**, 5293 (1999).
[20] A.V. Filinov, M. Bonitz, and Yu.E. Lozovik, Phys. Rev. Lett. **86**, 3851 (2001).
[21] I.V. Schweigert, V.A. Schweigert, and F.M. Peeters, Phys. Rev. Lett. **84**, 4381 (2000).
[22] Y.J. Lai and L. I, Phys. Rev. E **64**, 015601 (2001).
[23] L. Cândido, P. Phillips, and D.M. Ceperley, Phys. Rev. Lett. **86**, 492 (2001).
[24] A. Pertsinidis and X.S. Ling, Nature (London) **413**, 147 (2001).
[25] M.A. Moore and A. Pĕrez-Garrido, Phys. Rev. Lett. **82**, 4078 (1999).
[26] N. Metropolis, A.W. Rosenbluth, M.N. Rosenbluth, A.M. Teller, and E. Teller, J. Chem. Phys. **21**, 1087 (1953).
[27] R.C. Gann, S. Chakravarty, and G.V. Chester, Phys. Rev. B **20**, 326 (1979).

[28] S. Fortune, Algorithmica **2**, 153 (1987).
[29] For example, see F. M. Peeters, in *Two-Dimensional Electron Systems*, edited by E. Y. Andrei (Kluwer Academic, Dordrecht, The Netherlands, 1997), p. 17.
[30] A.A. Koulakov and B.I. Shklovskii, Phys. Rev. B **57**, 2352 (1998).
[31] K.J. Strandburg, Rev. Mod. Phys. **60**, 161 (1988); J.G. Dash, *ibid.* **71**, 1737 (1999).
[32] V.M. Bedanov, G.V. Gadiyak, and Yu.E. Lozovik, Phys. Lett. **109A**, 289 (1985).
[33] B.I. Halperin and D.R. Nelson, Phys. Rev. Lett. **41**, 121 (1978).